



1 **Impact of anticyclonic eddies on the spatial distribution**
2 **and emission of non-methane hydrocarbons in the**
3 **northern South China Sea**

4 Zhen-Fei Liu^{1,2}, Wen-Zhu Qiao³, Ze-Yun Yang¹, Feng Xu¹, Gao-Bin Xu¹, Jian Wang¹,
5 Hao Qiao¹, Cheng-Shuai Li¹, Hong-Hai Zhang^{1,2}

6 ¹Frontiers Science Center for Deep Ocean Multispheres and Earth System, Key Laboratory of Marine
7 Chemistry Theory and Technology, Ministry of Education, Ocean University of China, Qingdao 266100,
8 China

9 ²Laoshan Laboratory, Qingdao 266237, China

10 ³Weihai Institute of Product Quality Standard and Metrology Inspection, Weihai 264209, China

11 *Correspondence to:* Jian Wang (wangjian@ouc.edu.cn) and Hong-Hai Zhang
12 (honghaizhang@ouc.edu.cn)

13 **Abstract.** Non-methane hydrocarbons (NMHCs) are important trace active gases that exert significant
14 impacts on climate. Ubiquitous mesoscale eddies likely act as a key physical process regulating the
15 marine emission of these gases, yet the underlying mechanisms remain poorly understood. Herein, we
16 characterized the distributions and emissions of NMHCs in the South China Sea, with particular
17 emphasis on the impacts of an anticyclonic eddy. Significantly lower NMHC concentrations were
18 observed within the eddy-controlled region ($201 \pm 101 \text{ pmol L}^{-1}$) relative to the reference sites ($433 \pm$
19 62.5 pmol L^{-1}). Downwelling in the anticyclonic eddy core reduced surface nutrient availability,
20 suppressing the biological production and surface concentrations of alkanes and isoprene, whereas lower
21 alkene levels were mainly driven by weakened photochemical production. NMHC sea-to-air fluxes
22 dropped by 56% within the eddy, which further diminished ozone and secondary organic aerosol
23 generation by 59% and 60%, respectively. Overall, our findings elucidate the regulatory role of mesoscale
24 eddies in NMHC dynamics, highlighting their critical function in shaping marine trace gas cycling and
25 associated environmental consequences.

26 **1 Introduction**

27 Non-methane hydrocarbons (NMHCs) represent a key subgroup of volatile organic compounds
28 (VOCs) that can exert substantial influences on atmospheric reactivity and global climate patterns (Yuan



29 et al., 2018). Atmospheric NMHCs can participate in reactions with hydroxyl radicals (OH) and
30 significantly contribute to tropospheric ozone (O₃) production (Atkinson, 2000; Tran et al., 2013). In
31 addition, NMHCs act as essential precursors to secondary organic aerosols (SOA) formation that
32 ultimately impact climate forcing and regional air pollution through cloud condensation nuclei generation,
33 thereby modifying radiation budgets and atmospheric quality (Hallquist et al., 2009; Carpenter et al.,
34 2012; Ding et al., 2013; Krechmer et al., 2015; Riva et al., 2016).

35 NMHCs have diverse sources, which can be categorized as anthropogenic and natural sources. Key
36 anthropogenic contributions arise from activities such as biomass burning, vehicular emissions, and
37 various industrial operations (Song et al., 2018, 2020), while natural sources comprise emissions by
38 terrestrial plants and marine phytoplankton (Luo and Yu, 2010; Messina et al., 2016). As a primary global
39 reservoir of organic carbon, the ocean is an important natural emission source of NMHCs. Phytoplankton
40 production is considered the principal source of marine dissolved isoprene, and phytoplankton can also
41 produce other NMHCs such as ethane, propane, ethene, and propene (McKay et al., 1996; Broadgate et
42 al., 2004; Dani and Loreto, 2017). Additionally, it has been demonstrated that photodegradation of marine
43 dissolved organic matter (DOM) is another important pathway for NMHC generation (Lee and Baker,
44 1992; Tran et al., 2013). The photochemical production rate of NMHCs was not only related to the
45 concentration of DOM, but also to its activity, light intensity, and radiation wavelength (Ratte et al.,
46 1998). The removal of NMHCs from seawater occurs through three main mechanisms: sea-to-air
47 exchange, microbial degradation, and hydrochemical reactions, with sea-to-air emission identified as the
48 principal removal pathway for oceanic NMHCs (Gist and Lewis, 2006). Global oceanic NMHC fluxes
49 are estimated at 2–50 Tg C yr⁻¹ (Tran et al., 2013), exerting substantial impacts on atmospheric chemical
50 processes within the marine boundary layer.

51 As a ubiquitous physical process throughout the global ocean, mesoscale eddies critically modulate
52 circulation patterns and dynamical regimes through energy cascades and material transport
53 (McGillicuddy, 2016). It is well established that mesoscale eddies significantly influence ocean
54 biogeochemistry (McGillicuddy et al., 1998; Dai et al., 2020; Liu et al., 2020; Zhang et al., 2023; Zhou
55 et al., 2023). Mesoscale eddies are categorized as anticyclonic, cyclonic, or mode-water eddies according
56 to the vertical displacement (subsidence or uplift) of the main and seasonal thermoclines (McGillicuddy



57 et al., 2007). Generally, anticyclonic eddies can enhance water column stratification and limit upward
58 nutrient replenishment, resulting in diminished primary productivity (Shih et al., 2020). Conversely, by
59 driving upwelling and transporting subsurface nutrients to the euphotic zone, cyclonic eddies may
60 enhance primary productivity and reshape phytoplankton community dynamics (Zhou et al., 2020; An et
61 al., 2024). Therefore, mesoscale eddies can significantly modulate phytoplankton productivity within the
62 euphotic zone and influence DOM concentrations and their associated carbon export flux (Zhou et al.,
63 2013, 2020; Liang et al., 2025). Given their pronounced impacts on phytoplankton dynamics and DOM
64 cycling, mesoscale eddies are likely key regulators of NMHC spatial distribution patterns and emissions.
65 However, due to constrained observations, the quantitative understanding of these effects remains limited
66 and fragmented, and the relevant mechanisms are unclear.

67 The South China Sea (SCS) is the largest semi-enclosed marginal sea in the western Pacific Ocean.
68 The Asian monsoon system drives a distinct seasonal wind reversal over the SCS, with prevailing
69 southwesterlies in summer and northeasterlies in winter. Influenced by the monsoon, Kuroshio waters
70 intrude into the SCS through the Luzon Strait, and the invading Kuroshio branch can lead to seasonal
71 shedding of eddy (Jia and Chassignet, 2011). The combined influences of monsoonal forcing, Kuroshio
72 intrusion, and intricate seabed topography (Men et al., 2024) render the SCS (especially the northern
73 SCS) an area of intense eddy activity (Lin et al., 2015), establishing it as a key region for investigating
74 mesoscale ocean processes. Here, we systematically investigated NMHC spatial distributions and
75 emissions in northeastern SCS, specifically focused on their response to an anticyclonic eddy. By further
76 assessing the contribution of NMHCs to O₃ formation and SOA production, we evaluate the potential
77 climate effects induced by mesoscale eddies through their modulation of oceanic NMHC fluxes. This
78 work provides new insights into the pivotal function of mesoscale eddies in regulating NMHC
79 biogeochemical cycles.

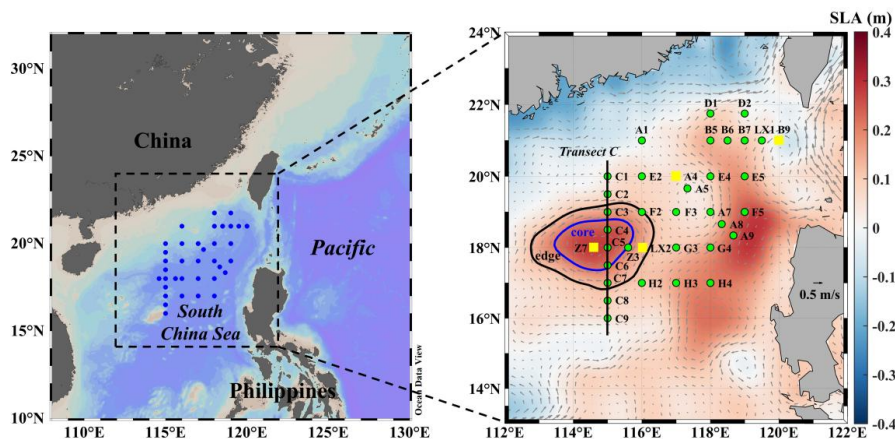
80 **2 Materials and methods**

81 **2.1 Cruise and sampling**

82 The cruise was conducted in the northern SCS on board the R/V "*Dongfanghong 3*" from 21 August
83 to 4 September 2021. The study area and sampling locations are shown in Fig. 1. Seawater samples were



84 collected from 36 stations, including 9 vertical stations along transect C. The survey period revealed
 85 marked positive sea surface height elevations localized in the southeastern and western areas of the
 86 sampling domain. Further analysis incorporating surface geostrophic currents revealed that a relatively
 87 regular-shaped anticyclonic eddy (AE) was present in the west of the study area, while the sea level
 88 anomaly (SLA) in the southeastern region lacked the typical structural characteristics of an eddy and was
 89 therefore not classified as an anticyclonic eddy. The AE formed through the eddy merger at the end of
 90 July and eventually dissipated in early November, spanning a lifespan of about 100 days. According to
 91 established eddy stage classifications defined by lifespan (Sweeney et al., 2003), AE was sampled at the
 92 end of its intensification.



93
 94 **Figure 1.** Map of sampling stations based on the sea level anomaly (SLA) and surface geostrophic current on 21
 95 August 2021. Yellow squares indicate the stations for incubation experiments. Transect C that cutting through the
 96 core of anticyclonic eddy (AE) was chosen to analyze the sectional distributions of NMHCs. The data for SLA and
 97 surface geostrophic current were obtained from Copernicus Marine Service (<https://marine.copernicus.eu>).

98 After collection using Niskin bottles (12 L) mounted on a conductivity–temperature–depth (CTD, Sea-
 99 Bird 911) rosette, seawater was subsampled into clear glass vials (120 mL). To assess analytical
 100 variability, duplicate samples were collected at approximately 10% of the stations (n = 4). To inhibit
 101 biological activity, samples were preserved by adding 100 μL of saturated HgCl_2 solution. These vials
 102 were then sealed without headspace and placed in a dark environment at 4 $^\circ\text{C}$ for subsequent NMHC
 103 determination (Wu et al., 2021, 2023). All samples were delivered to the shore-based laboratory and
 104 analyzed within one month. It has been reported that the concentrations of NMHCs in sample vials
 105 showed no significant variation over a period of two months (Zhang et al., 2015).



106 **2.2 Analysis of NMHCs**

107 Seawater NMHCs were determined via a purge-and-trap system coupled to a gas chromatography-
108 mass spectrometer (GC-MS, 8860/5977B, Agilent, USA). The target compounds of eight light NMHC
109 species included ethane, propane, i-butane, n-butane, ethene, propene, i-butene, and isoprene. For
110 analysis, a 100 mL sample was purged for 15 min in the extraction chamber by bubbling with pure helium
111 flowing at 80 mL min⁻¹. To eliminate water vapor and carbon dioxide, the gas stream was purified using
112 magnesium perchlorate and sodium hydroxide granules, and subsequently trapped in a liquid nitrogen-
113 cooled stainless-steel trap. Following thermal desorption with boiling water, the released NMHCs were
114 injected into the GC-MS. Separation and quantification were achieved using the Rt-Alumina BOND/KCl
115 capillary column (30 m × 0.32 mm × 5 μm, Restek, USA). The NMHC standard gas (nominal
116 concentration: 1.00 ppmv in helium, Linde Gas, Germany) was diluted with pure helium to prepare
117 working standards at concentrations of 1, 5, 10, 20, 50, and 100 ppbv. Calibration curves were
118 constructed by plotting the peak area against the concentration of each compound, and linear regression
119 was applied. The correlation coefficients (R²) for all target compounds exceeded 0.99. The method
120 detection limits (signal-to-noise ratio of 3) for the eight NMHC species ranged from 0.5 to 1.0 pmol L⁻¹,
121 with precisions (evaluated by analyzing six replicate standards at two concentration levels: 22.3 and 89.3
122 pmol L⁻¹) between 3% and 6% (see Table S1 for details).

123 **2.3 Analysis of environmental parameters**

124 For Chl-*a* analysis, the seawater samples (1 L) were filtered through GF/F membranes (0.7 μm,
125 Whatman, UK). After folding, membranes were transferred into 15 mL sterilized plastic tubes wrapped
126 in tinfoil, and maintained frozen (-20 °C) until analysis. Extraction of Chl-*a* was performed by adding
127 10 mL of 90% (v/v) acetone solution into plastic tubes. After 24 h at 4 °C, the samples were centrifuged
128 to obtain supernatant, and the fluorescence intensity of the supernatant was determined with a
129 fluorescence spectrophotometer (F-4700, Hitachi, Japan). For dissolved organic carbon (DOC) analysis,
130 the filtrates (30 mL) filtered by GF/F membranes were collected in precombusted (450 °C overnight)
131 brown-colored glass vials, and the concentration of DOC was determined with a total organic carbon
132 analyzer (TOC-VCPH, Shimadzu, Japan). For nutrient analysis, the filtrates (50 mL) filtered by GF/F
133 membranes were collected in polyethylene bottles. The concentrations of dissolved inorganic nitrogen



134 (DIN, nitrate + nitrite), silicate, and phosphate were determined with an automatic analyzer (AA3, Seal,
135 Germany). Seawater salinity and temperature were measured using a CTD instrument cluster, while the
136 data on wind speed were recorded by the shipboard meteorological station (AWS430, Vaisala, Finland)
137 installed on the scientific mast at the foremost deck at ~10 m above the sea surface.

138 **2.4 Deck incubation experiments**

139 Seawater sampled from a 5 m depth using Niskin bottles at 4 stations (A4, B9, Z3, and Z7) for NMHC
140 photochemical production rate experiments. To exclude phytoplankton and microbes, seawater was
141 subjected to filtration through polyethersulfone membranes (0.2 μm , PALL, USA). The filtrates were
142 then slowly dispensed into sterile quartz tubes (180 mL, 4 cm in diameter, 15 cm in length) and sealed
143 with screw caps equipped with PTFE-faced silicone septa to ensure no headspace. These quartz tubes
144 were subjected to four distinct light treatments: (i) unwrapped to receive full-spectrum solar radiation;
145 (ii) wrapped with Mylar-D film to transmit radiation in the photosynthetically active radiation (PAR,
146 400–700 nm) and ultraviolet A (UVA, 320–400 nm) spectral bands; (iii) wrapped with UF3 Plexiglas to
147 nearly exclusively transmit radiation in PAR spectral bands; and (iv) wrapped with at least three layers
148 of tinfoil to serve as dark controls. For each sampling station, three replicate quartz tubes were prepared
149 for each light treatment. These quartz tubes were subjected to incubation under natural solar radiation in
150 a water bath on the ship's deck. To maintain in situ temperature, the bath was continuously flushed with
151 surface seawater. Incubations were carried out over a 6-hour period (09:00–15:00 local time) to capture
152 the peak intensity of solar radiation. The photochemical production rate was calculated by dividing the
153 increase in NMHC concentration by the incubation time. Furthermore, NMHC photochemical production
154 rates in the PAR, ultraviolet B (UVB, 280–320 nm), and UVA spectral ranges can be estimated by
155 comparing the differences in production rates among the four light-treatment groups. The filtered
156 seawater was assumed to be virus-containing with low microbial biomass, while phytoplankton were
157 effectively removed (Ratte et al., 1993). Given the current lack of clarity and relevant studies regarding
158 the role of viruses in NMHC production and consumption, their potential impact on NMHC dynamics in
159 seawater was not considered in this study. It should be noted that photodegradation of NMHCs may have
160 occurred during the light incubation, and this potential loss process was not quantitatively assessed in



161 this work. Thus, the measured photochemical production of NMHCs represents net values, which may
162 include an unquantified component of photodegradation.

163 2.5 Calculation of sea-to-air fluxes

164 The sea-to-air fluxes (F , $\text{nmol m}^{-2} \text{d}^{-1}$) of NMHCs were calculated according to Eq. (1):

$$165 \quad F = k \times (C_w - C_a \times H) \quad (1)$$

166 where k (cm h^{-1}) is the gas transfer velocity; C_w (pmol L^{-1}) is the seawater NMHC concentration; C_a
167 (pptv) is the atmospheric NMHC mixing ratio; and H (M atm^{-1}) is Henry's law constant. Due to the
168 highly supersaturated levels of light NMHCs in surface seawater compared to the atmosphere (exceeding
169 one order of magnitude), atmospheric NMHCs can be considered negligible (Plass-Dülmer et al., 1993);
170 thus, Eq. (1) can be simplified to:

$$171 \quad F = k \times C_w \quad (2)$$

172 The gas transfer velocity was calculated following the method of Wanninkhof (2014), as shown in Eq.
173 (3):

$$174 \quad k = 0.251 \times u^2 \times (S_C/660)^{-0.5} \quad (3)$$

175 where u (m s^{-1}) is the wind speed at 10 m above the sea level. The Schmidt number S_C is given by the
176 ratio $S_C = \mu / D$, where μ ($\text{cm}^2 \text{s}^{-1}$) is the kinematic viscosity of seawater (Wanninkhof, 1992) and D is
177 the diffusion coefficient of the considered species (Wilke and Chang, 1955).

$$178 \quad \mu = 1.052 + 1.300 \times 10^{-3} \times t + 5.000 \times 10^{-6} \times t^2 - 5.000 \times 10^{-7} \times t^3 \quad (4)$$

$$179 \quad D = 7.4 \times 10^{-8} \times (q \times M_b)^{0.5} \times T / (n_b \times V_a^{0.6}) \quad (5)$$

180 where t ($^{\circ}\text{C}$) is the seawater temperature in Celsius; q is the association factor of water with the value of
181 2.6; M_b (g mol^{-1}) is the molar weight of water; T (K) is the seawater temperature in Kelvin; n_b is the
182 dynamic viscosity of seawater, and V_a is the molar volume at boiling point.

183 2.6 Assessment of NMHC environmental effects

184 A key process governing the chemical transformation of NMHCs in the troposphere is their reaction
185 with OH. The reactivity of individual NMHCs is quantified by Eq. (6):

$$186 \quad L_{i,OH} = \text{NMHC}_i \times k_{i,OH} \quad (6)$$



187 where $L_{i,OH}$ (s^{-1}) is the OH consumption rate of NMHCs; $NMHC_i$ ($mol\ m^{-3}$) is the concentration of
188 atmospheric NMHCs; and $k_{i,OH}$ ($cm^3\ molecule^{-1}\ s^{-1}$) is the constant for NMHCs reacting with OH (Carter,
189 2010).

190 NMHC species with greater chemical reactivity are associated with larger contributions to atmospheric
191 O_3 and SOA production (Panda et al., 2015). The role of each NMHC in O_3 and SOA formation was
192 assessed through the respective calculation of their O_3 formation potential (OFP , $\mu g\ m^{-3}$) and SOA
193 formation potential (P_{SOAP} , $\mu g\ m^{-3}$) via Eq. (7) and (8).

$$194 \quad OFP_i = NMHC_i \times MIR_i \quad (7)$$

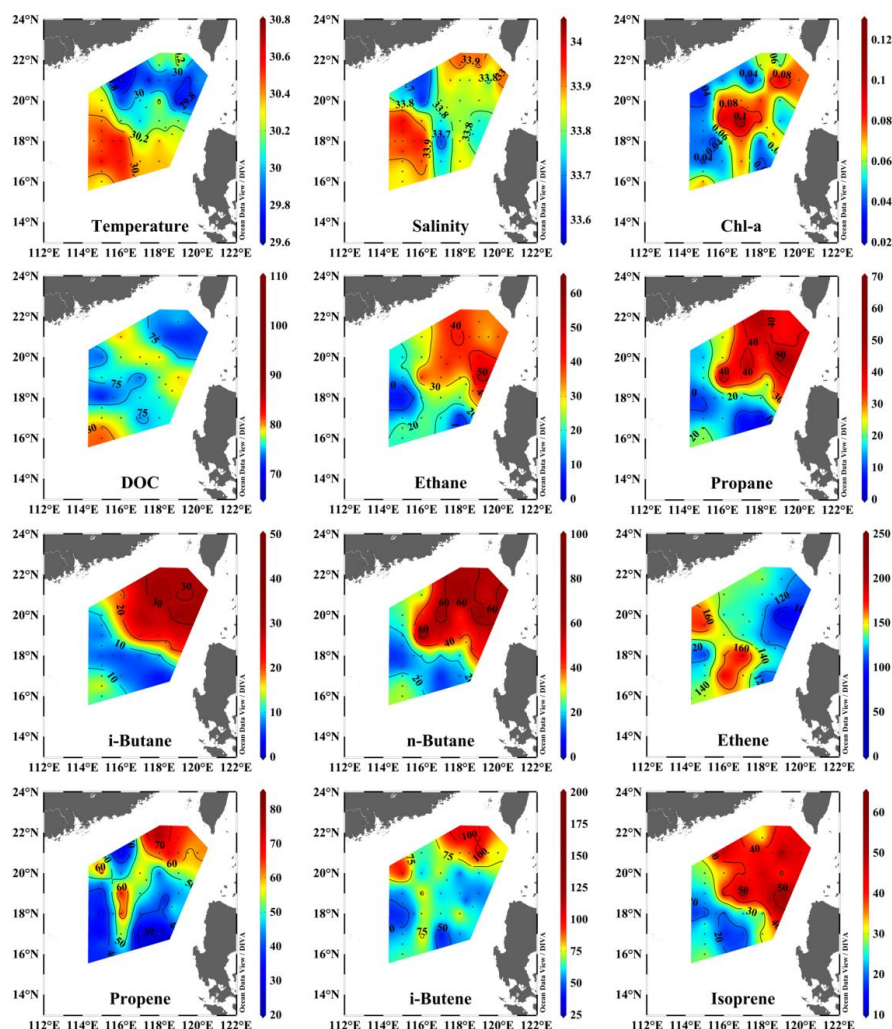
$$195 \quad P_{SOAP_i} = NMHC_i \times SOAP_i \times FAC_{toluene} \quad (8)$$

196 where $NMHC_i$ ($mol\ m^{-3}$) is the concentration of atmospheric NMHCs; MIR_i ($g\ O_3/g\ VOC$) is the
197 maximum O_3 increment reactivity (Carter, 2010); $SOAP_i$ is the tendency (relative to toluene = 100) of
198 each NMHC to form SOA (Derwent et al., 2010); and $FAC_{toluene}$ is the fractional aerosol coefficient of
199 toluene, which has a value of 5.4% (Zhang et al., 2017).

200 **3 Results**

201 **3.1 Hydrographic characteristics**

202 Spatial distributions of temperature, salinity, Chl-*a*, and DOC in surface seawater of the northern SCS
203 obtained during the cruise are shown in Fig. 2. The mean (range) of surface temperature and salinity
204 across the survey area were 30.20 ± 0.31 (29.59 – 30.71) °C and 33.84 ± 0.11 (33.59 – 34.01), respectively.
205 The high-temperature region corresponded to areas with elevated SLA, with the highest temperatures
206 (30.54 ± 0.12 °C) observed within the AE. Additionally, sea surface salinity was also relatively high
207 within the area controlled by the AE. Based on the SLA and K-means cluster analysis (Tian et al., 2025),
208 the sampling stations were classified into three categories: eddy core, eddy edge, and reference sites.
209 Detailed SLA values and station classifications were provided in Table S2.



210

211 **Figure 2.** Horizontal distributions of temperature (°C), salinity, Chl-*a* ($\mu\text{g L}^{-1}$), DOC ($\mu\text{mol L}^{-1}$), and NMHCs (pmol L^{-1}) in surface seawater of the northern SCS.

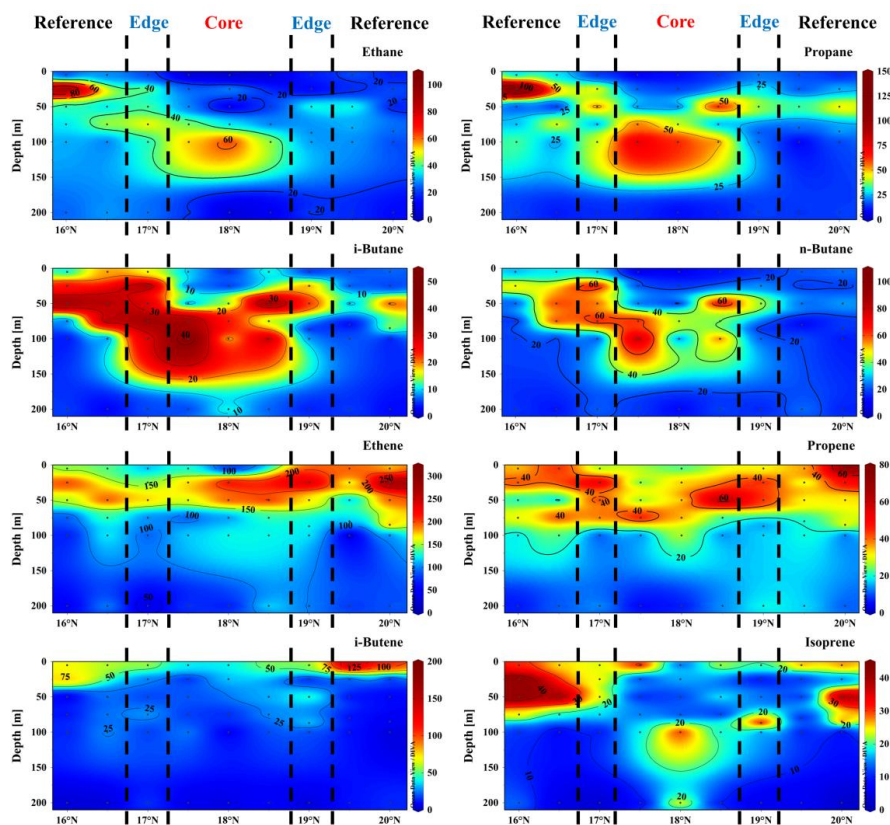
213 The surface Chl-*a* concentration ranged from 0.02 to 0.12 $\mu\text{g L}^{-1}$, averaging $0.06 \pm 0.02 \mu\text{g L}^{-1}$, and
 214 exhibited clear modulation by the AE. A relatively high Chl-*a* concentration was observed in the
 215 northeastern sector of the study area, with an average of $0.07 \pm 0.02 \mu\text{g L}^{-1}$. In contrast, Chl-*a*
 216 concentrations were lowest within the AE, with an average of $0.04 \pm 0.01 \mu\text{g L}^{-1}$, representing a 39.6%
 217 decrease compared to the reference sites (*t*-test: $t = 3.090$, $p = 0.005$). Similarly, the distribution of DOC
 218 was also influenced by the AE, with lower values in the core of AE ($72.17 \pm 9.62 \mu\text{mol L}^{-1}$) and higher
 219 concentrations at the reference sites ($80.48 \pm 8.94 \mu\text{mol L}^{-1}$).



220 3.2 Spatial variability of seawater NMHCs

221 The concentrations of ethane, propane, i-butane, n-butane, ethene, propene, i-butene, and isoprene in
222 surface seawater ranged from 1.0–64.4, 0.7–67.7, 0.8–49.8, 4.4–99.2, 3.5–239, 21.3–85.0, 32.0–175, and
223 10.4–64.8 pmol L⁻¹, with mean values of 26.7 ± 15.4, 26.1 ± 17.4, 19.5 ± 13.6, 37.3 ± 25.1, 129 ± 47.1,
224 48.6 ± 19.3, 69.7 ± 30.3, and 34.1 ± 15.3 pmol L⁻¹, respectively. Alkenes accounted for a relatively large
225 proportion of total NMHCs, with concentrations being 85.8%–383% higher than those of alkanes with
226 the same carbon number. The distribution of NMHCs was also significantly influenced by the eddy, with
227 their mean concentrations in the AE-dominated area (201 ± 101 pmol L⁻¹) being notably lower than those
228 at the reference sites (433 ± 62.5 pmol L⁻¹) (*t*-test: *t* = 5.645, *p* < 0.001). However, distinct distribution
229 patterns were observed among different species. Alkanes and isoprene exhibited similar horizontal
230 distribution patterns, with elevated values mainly occurring in the central and northeastern regions that
231 were unaffected by the AE. In contrast, the concentrations of alkanes and isoprene in the region controlled
232 by the AE were markedly lower, accounting for only 36.5%–57.9% of the regional average. For C₂–C₄
233 alkenes, elevated values were observed not only in the northeastern sector but also along the eddy edge.
234 However, their concentrations observed within the eddy core were substantially reduced, representing a
235 25.5%–37.8% decrease relative to the regional mean. Overall, the mean concentrations of all NMHC
236 components at the AE were significantly reduced relative to the reference sites (*t*-test: *t* = 2.132–5.208,
237 *p* < 0.05; see Table S3).

238 Transect C crossing through the center of AE shows the vertical profiles of NMHCs (Fig. 3). Within
239 the eddy core, the isolines of alkanes and isoprene displayed a pronounced downward displacement. In
240 the upper 0–50 m layer of the eddy core, their concentrations were markedly depleted compared to the
241 eddy edge and reference sites. Their maximum concentrations were observed below 100 m within the
242 eddy core, whereas at the reference sites, high values generally occurred above 50 m. Unlike alkanes and
243 isoprene, the maximum values of C₂–C₄ alkenes did not exhibit a downward shift at the core of AE.



244
245 **Figure 3.** Vertical profiles of NMHCs (pmol L^{-1}) along transect C in the northern SCS.

246 **3.3 Photochemical production rates of NMHCs**

247 Photochemical production was considered an important source of marine NMHCs. In seawater filtered
248 through $0.2 \mu\text{m}$ membranes to remove microorganisms and particles, the concentrations of NMHCs
249 increased after 6 hours of solar irradiation (Fig. S1). $\text{C}_2\text{-C}_4$ alkenes exhibited the largest enhancement,
250 with increases of 63%–210%, far exceeding the changes observed for other compounds. The
251 photochemical production rates of ethane, propane, i-butane, n-butane, ethene, propene, i-butene, and
252 isoprene ranged from 2.5–3.1, 4.3–4.4, 2.4–3.4, 4.0–7.0, 24.1–38.8, 5.3–22.9, 12.2–15.3 and 2.6–4.7
253 $\text{pmol L}^{-1} \text{h}^{-1}$, with mean values of 2.8 ± 0.4 , 4.4 ± 0.1 , 2.9 ± 0.7 , 5.5 ± 2.2 , 32.2 ± 6.2 , 18.1 ± 8.6 , $13.8 \pm$
254 1.7 , and $3.7 \pm 1.5 \text{ pmol L}^{-1} \text{h}^{-1}$, respectively. Photochemical production rates of $\text{C}_2\text{-C}_4$ alkenes were 4–
255 11 times higher than those of alkanes with the same carbon number, indicating that alkenes are the
256 dominant photochemical products (Fig. S1). In addition, the photochemical production rates of $\text{C}_2\text{-C}_4$



257 alkenes showed substantial spatial variability. The rates of ethene, propene, and i-butene in the eddy core
 258 (24.1, 5.3, and 12.2 pmol L⁻¹ h⁻¹, respectively) were significantly lower than those at the eddy edge
 259 (ethene: 34.6 pmol L⁻¹ h⁻¹; propene: 21.5 pmol L⁻¹ h⁻¹; i-butene: 15.3 pmol L⁻¹ h⁻¹) and at the reference
 260 sites (ethene: 35.0 ± 5.4 pmol L⁻¹ h⁻¹; propene: 22.8 ± 0.2 pmol L⁻¹ h⁻¹; i-butene: 13.9 ± 2.1 pmol L⁻¹
 261 h⁻¹) (Table 1). Moreover, photochemical production rates differed markedly among individual C₂–C₄
 262 alkenes, and the relative contributions of individual spectral bands varied accordingly. The contributions
 263 of different radiation bands to the photochemical production of C₂–C₄ alkenes followed the order UVB >
 264 UVA > PAR, with the UVB band accounting for the majority of photochemical production and
 265 contributing up to 71.3%.

266 **Table 1.** The photochemical production rate of C₂–C₄ alkenes (full-spectrum solar radiation, as well as UVB, UVA,
 267 and PAR spectral bands), and the contribution percentage of different radiation bands.

Category	Station	Specie	Photochemical production rate (pmol L ⁻¹ h ⁻¹)				Contribution percentage (%)		
			natural light	UVB	UVA	PAR	UVB	UVA	PAR
Eddy Core	Z7	Ethene	24.1	17.1	6.1	0.8	71.3	25.4	3.3
		Propene	5.3	2.5	1.9	0.9	47.4	35.6	16.7
		i-Butene	12.2	7.7	3.0	1.5	63.4	24.4	12.2
Eddy Edge	LX2	Ethene	34.6	25.4	7.1	2.1	73.4	20.7	5.9
		Propene	21.5	13.0	6.3	2.2	60.4	29.3	10.4
		i-Butene	15.3	6.5	6.3	2.5	42.7	41.1	16.2
Reference Site	A4	Ethene	38.8						
		Propene	22.6						
		i-Butene	12.4						
Reference Site	B9	Ethene	31.2						
		Propene	22.9						
		i-Butene	15.3						

268 **4 Discussion**

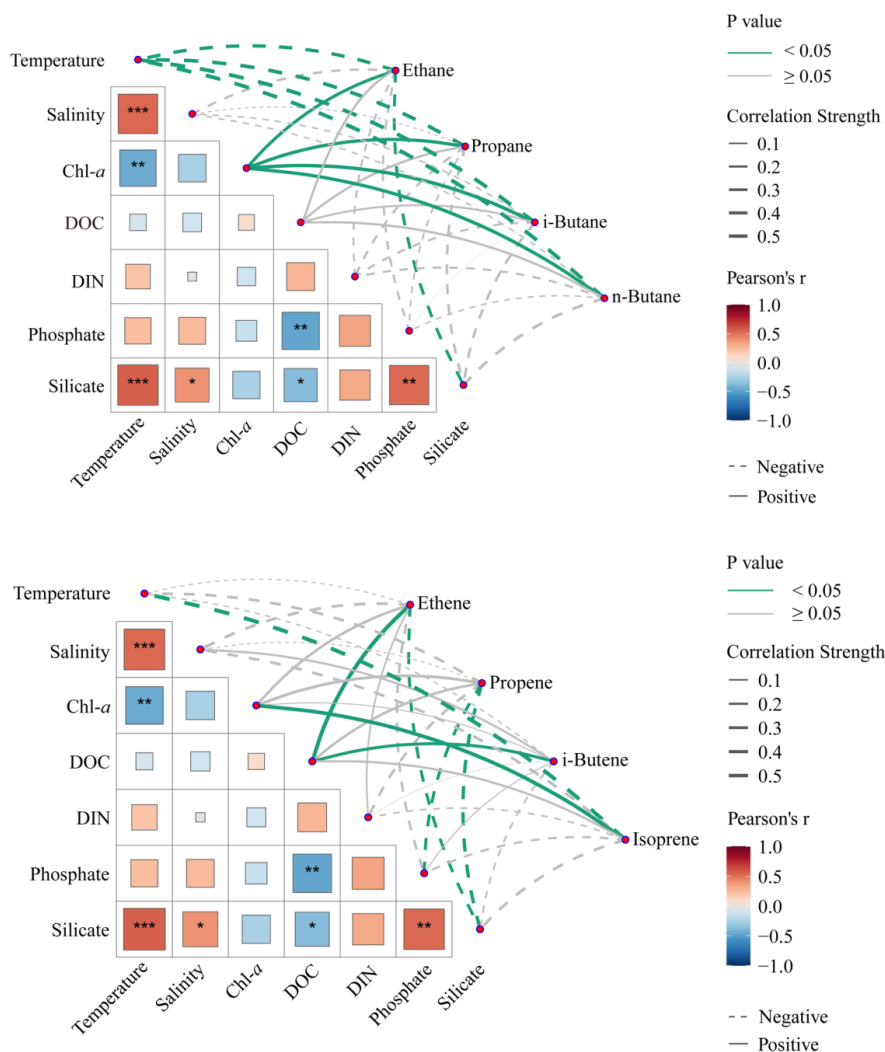
269 **4.1 Biological controls of alkanes and isoprene under anticyclonic eddy–induced stratification**

270 Anticyclonic eddies are characterized by enhanced upper-ocean stratification and strong water-column
 271 convergence, as indicated by the pronounced downward deflections of isotherms and isopycnals in the
 272 eddy core (Fig. S2). These physical processes substantially modify the vertical distributions of dissolved



273 nutrients and phytoplankton biomass. Surface nutrients were nearly undetectable within the AE, but
274 increased gradually with depth. Notably, below 75 m, nutrient concentrations in the eddy core (DIN: 5.84
275 $\pm 3.55 \mu\text{mol L}^{-1}$; phosphate: $0.29 \pm 0.22 \mu\text{mol L}^{-1}$) were significantly lower than those at the eddy edge
276 (DIN: $11.75 \pm 0.35 \mu\text{mol L}^{-1}$; phosphate: $0.67 \pm 0.13 \mu\text{mol L}^{-1}$) and reference sites (DIN: 11.15 ± 1.62
277 $\mu\text{mol L}^{-1}$; phosphate: $0.52 \pm 0.07 \mu\text{mol L}^{-1}$) (ANOVA test, $p < 0.05$), likely reflecting suppressed upward
278 nutrient fluxes under strong convergence in the eddy core. As a consequence of nutrient limitation, the
279 deep chlorophyll maximum (DCM) was displaced downward to ~ 100 m in the eddy core, markedly
280 deeper than the ~ 75 m observed at the reference sites and the eddy edge. Moreover, Chl-*a* concentrations
281 within the DCM layer of the eddy core ($0.25 \pm 0.11 \mu\text{g L}^{-1}$) were substantially lower than those at the
282 eddy edge ($0.31 \pm 0.09 \mu\text{g L}^{-1}$) and reference sites ($0.34 \pm 0.06 \mu\text{g L}^{-1}$). These results indicate that
283 anticyclonic eddy dynamics inhibit phytoplankton growth by enhancing stratification and restricting
284 nutrient supply to the euphotic zone.

285 Given that phytoplankton are important biological sources of short-chain alkanes and isoprene
286 (McKay et al., 1996; Wang et al., 2023), the suppression of phytoplankton biomass within the AE is
287 expected to reduce the biological production of these NMHCs. This explains the lower surface
288 concentrations of alkanes and isoprene in the core of AE, as well as their pronounced downward
289 displacement in the vertical profiles. This mechanistic interpretation is supported by correlation analysis
290 (Fig. 4). Ethane, propane, i-butane, n-butane, and isoprene were significantly intercorrelated ($r = 0.508$ –
291 0.968 , $n = 36$, $p < 0.01$) and also showed significant positive correlations with Chl-*a* ($r = 0.403$ – 0.544 , n
292 $= 36$, $p < 0.05$), indicating a common biological control. Overall, anticyclonic eddies declined the nutrient
293 supply to influence phytoplankton growth, thereby modulating the biological production and spatial
294 distributions of alkanes and isoprene.



295

296 **Figure 4.** Pearson correlation matrices for environmental parameters and NMHCs in surface seawater, with line
 297 thickness and color indicating the strength of the Pearson correlation coefficient (r) and significance (p -value).

298 **4.2 Eddy-driven changes in alkene photochemical production and their wavelength-dependence**

299 The photochemical production rates of C_2 – C_4 alkenes varied significantly among stations. However,
 300 because the zonal extent of the study region was only 4° , the variations in solar irradiance among stations
 301 during the incubation period were minimal (852 – 895 W m^{-2}), which was insufficient to explain the inter-
 302 station differences. Instead, the spatial variability in photochemical production was likely controlled by
 303 the availability of photoreactive substrates. Research has indicated that DOC serves as a key substrate



304 for seawater alkenes photoproduction, and its concentrations play an important role in determining alkene
305 production (Ratte et al., 1998). DOC concentrations at the eddy core (Z7: 62.61 $\mu\text{mol L}^{-1}$) were markedly
306 lower than those at the eddy edge (LX2: 89.83 $\mu\text{mol L}^{-1}$) and the reference sites (A4: 95.50 $\mu\text{mol L}^{-1}$;
307 B9: 84.58 $\mu\text{mol L}^{-1}$). Thus, limited DOC availability within the AE restricted the photochemical
308 formation of C₂–C₄ alkenes, ultimately leading to the lower alkene concentrations inside the eddy. This
309 interpretation is further supported by the significant correlations between DOC and ethene ($r = 0.388$, n
310 $= 36$, $p < 0.05$)/i-butene ($r = 0.505$, $n = 36$, $p < 0.01$). DOC isopleths in vertical profiles showed a
311 downward displacement, with DOC concentrations at 75–100 m in the eddy core markedly higher than
312 those at the eddy edge and reference stations (Fig. S2). However, alkenes showed no comparable
313 distribution pattern, likely due to insufficient light limiting their photochemical production in deeper
314 water.

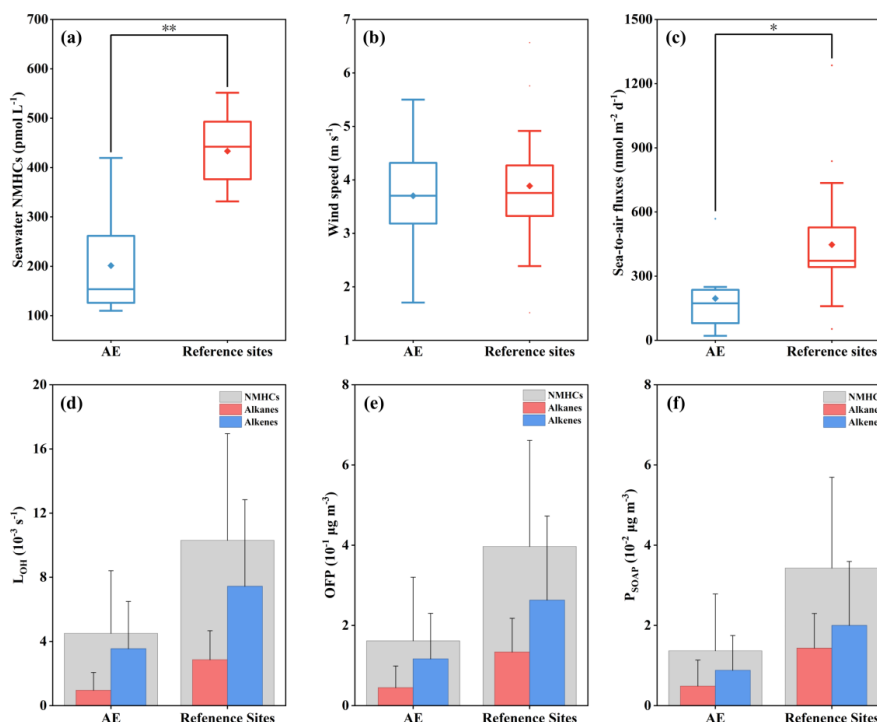
315 The relative energy distribution of incident solar radiation across PAR, UVA, and UVB is
316 approximately 90:11:1 (Bird and Riordan, 1986), and this spectral partitioning was used to normalize
317 alkene photochemical production rates to evaluate their wavelength-dependence, with ethene, propene,
318 and i-butene exhibiting UVB:UVA:PAR ratios of 1446:35:1, 707:21:1, and 665:23:1, respectively.
319 Although UVB represents only a small fraction of total solar radiation, its shorter wavelength and higher
320 photon energy are more effective at cleaving photolabile bonds within DOM, resulting in substantially
321 higher photochemical yields of C₂–C₄ alkenes.

322 4.3 Declined NMHC emissions and associated atmospheric effects within AE

323 Assessing the impact of NMHCs on global climate feedback requires precise estimates of their sea-to-
324 air exchange fluxes. The mean (range) of sea-to-air fluxes of ethane, propane, i-butane, n-butane, ethene,
325 propene, i-butene, and isoprene were 29.4 ± 30.1 (0.8–156), 26.5 ± 33.1 (0.2–184), 18.2 ± 23.1 (0.1–
326 125), 35.0 ± 44.0 (1.2–250), 146 ± 136 (3.0–689), 48.6 ± 45.1 (3.7–225), 60.6 ± 51.7 (8.6–224), and 28.0
327 ± 24.2 (1.5–132) $\text{nmol m}^{-2} \text{d}^{-1}$, respectively. These calculated values were comparable to those reported
328 in the northwestern Pacific Ocean (Li et al., 2019; Wang et al., 2023; Wu et al., 2023), but they were
329 lower than those documented for the Yellow Sea and the East China Sea (Li et al., 2021; Wu et al., 2021;
330 Qiao et al., 2023; Wang et al., 2024) (Table S4). The mean flux of alkenes over the entire study region
331 was $267 \pm 240 \text{ nmol m}^{-2} \text{d}^{-1}$, approximately 2.5 times higher than that of alkanes ($108 \pm 128 \text{ nmol m}^{-2}$



332 d^{-1} ; t -test: $t = 3.512$, $p = 0.001$). In addition, the sea-to-air fluxes of alkenes typically exceed those of
 333 alkanes with the same carbon number, corresponding to their respective seawater concentrations.



334
 335 **Figure 5.** Comparison of NMHC fluxes and associated environmental effects between eddy-influenced regions and
 336 reference sites. Box plots show the (a) NMHC concentrations in surface seawater, (b) wind speeds, and (c) sea-to-
 337 air fluxes of NMHCs at reference sites and AE-dominated regions. The box boundaries indicate the 25th, 50th
 338 (median), and 75th percentiles, respectively, while the mean is denoted by a solid diamond. * and ** indicate
 339 statistical significance at the $p < 0.05$ and $p < 0.01$ levels, respectively. Panels d, e, and f show the atmospheric OH
 340 consumption rate, O₃ formation potential, and SOA formation potential of ocean-emitted NMHCs.

341 The seawater NMHC concentration, wind speed, and sea-to-air fluxes of NMHCs at different regions
 342 are presented in Fig. 5 (a)–(c). The sea-to-air fluxes of NMHCs were significantly influenced by the AE.
 343 Higher fluxes were predominantly observed at the reference sites, in contrast to the lower values within
 344 the regions controlled by the AE. Since wind speed showed no significant differences among stations
 345 across different regions, the surface seawater NMHC concentrations were the primary controlling factor
 346 that led to the variability of sea-to-air fluxes. Calculations revealed a mean NMHC sea-to-air flux of 196
 347 ± 170 $\text{nmol m}^{-2} \text{d}^{-1}$ within the AE, representing a 56% reduction relative to the reference sites ($447 \pm$



348 289 nmol m⁻² d⁻¹; *t*-test: *t* = -2.720, *p* = 0.013), demonstrating that the presence of anticyclonic eddies
349 suppressed the release of NMHCs.

350 To estimate the oceanic contribution to atmospheric NMHCs, we utilized a simple box model with a
351 500 m boundary layer height (Dacre et al., 2007), with the assumption that the ocean was the sole source
352 of NMHCs. Based on the atmospheric lifetimes (Table 2) and sea-to-air flux of each NMHC, we
353 calculated their resultant atmospheric concentrations attributable to oceanic emissions. The mean
354 atmospheric concentration of NMHCs was 159 ± 166 pptv. Although alkenes exhibited higher sea-to-air
355 fluxes, alkanes possessed substantially longer atmospheric lifetimes than alkenes, resulting in
356 significantly higher atmospheric alkane concentrations that accounted for up to 90% of the total. Based
357 on the calculated atmospheric NMHC concentrations, we assessed their reactivity in the atmosphere and
358 evaluated their contributions to O₃ and SOA (Table 2).

359 The mean *L_{OH}* of ethane, propane, i-butane, n-butane, ethene, propene, i-butene, and isoprene were
360 0.69 ± 0.71, 0.63 ± 0.79, 0.43 ± 0.54, 0.82 ± 1.03, 3.28 ± 3.06, 1.11 ± 1.03, 1.39 ± 1.19, and 0.64 ± 0.55
361 (10⁻³ s⁻¹), respectively, with alkenes exhibiting *L_{OH}* values approximately 2.4 times higher than alkanes.
362 Despite the lower calculated atmospheric concentrations of alkenes relative to alkanes, alkenes exhibited
363 higher *L_{OH}* values, demonstrating their greater reactivity toward OH and highlighting their significance
364 as key reactive atmospheric species. Similarly, the mean *OFP* of NMHCs was 3.30 ± 3.16 (10⁻¹ μg m⁻³),
365 with alkenes contributing the majority, accounting for approximately 64 %. Despite their lower
366 atmospheric concentrations, alkenes generally exhibited higher *OFP* values than alkanes, indicating their
367 crucial role in O₃ formation. However, the *P_{SOAP}* of alkanes and alkenes were 1.27 ± 1.41 and 1.60 ± 1.54
368 (10⁻³ μg m⁻³), respectively, with both groups contributing almost equally to SOA formation.

369 Within the regions controlled by the AE, the reduced sea-to-air fluxes resulted in lower atmospheric
370 concentrations, leading to diminished *L_{OH}*, *OFP*, and *P_{SOAP}* values for both alkanes and alkenes compared
371 to the reference sites (Fig. 5 (d)–(f)). Relative to the reference sites, the O₃ and SOA formation potential
372 of NMHCs at the AE decreased by 59% and 60%, respectively, suggesting that the anticyclonic eddies
373 could substantially weaken the atmospheric environmental impacts of marine NMHCs.



374 **Table 2.** Sea-to-air flux, the calculated atmospheric lifetime based on the reaction with OH, the calculated atmospheric concentrations, OH consumption rates (L_{OH}), O_3 formation potential (OFP),
 375 and SOA formation potential (P_{SOAP}) of each NMHC.

Species	Sea-to-air flux ($\text{mmol m}^{-2} \text{d}^{-1}$)	Atmospheric lifetime ^a (d)	Calculated concentrations in the atmosphere (pptv)	L_{OH} (10^{-3} s^{-1})	OFP ($10^{-1} \mu\text{g m}^{-3}$)	P_{SOAP} ($10^{-3} \mu\text{g m}^{-3}$)
Ethane	29.4 (0.8–156)	78	101 (1.83–542)	0.69 (0.01–3.70)	0.38 (0.01–2.04)	0.73 (0.01–3.93)
Propane	26.5 (0.2–184)	18	21.2 (0.15–148)	0.63 (0.004–4.42)	0.21 (0.001–1.43)	–
i-Butane	18.2 (0.1–125)	9.1	7.42 (0.03–51.1)	0.43 (0.002–2.94)	0.24 (0.001–1.63)	–
n-Butane	35.0 (1.2–250)	8.2	12.8 (0.45–91.7)	0.82 (0.03–5.86)	0.38 (0.01–2.74)	0.54 (0.02–3.85)
Ethene	146 (3.0–689)	2.3	15.0 (0.24–70.8)	3.28 (0.05–15.51)	1.69 (0.03–7.98)	1.31 (0.02–6.22)
Propene	48.6 (3.7–225)	0.73	1.58 (0.12–7.34)	1.11 (0.08–5.13)	0.35 (0.03–1.61)	0.26 (0.02–1.19)
i-Butene	60.6 (8.6–224)	0.38	1.02 (0.14–3.78)	1.39 (0.20–5.16)	0.16 (0.02–0.60)	0.08 (0.01–0.31)
Isoprene	28.0 (1.5–132)	0.19	0.24 (0.01–1.11)	0.64 (0.03–2.98)	0.08 (0.004–0.36)	0.07 (0.004–0.35)

^a Assuming a 24-hour average OH concentration of 6×10^5 molecules cm^{-3} (Jobson et al., 1999) and employing OH reaction rate constants at 288 K from (Atkinson and Arey, 2003).

“–” indicates no data

376
377
378



379 **5 Conclusion**

380 Our study clarifies characteristic NMHC distribution and emission features associated with mesoscale
381 eddies in the northern South China Sea, and further elucidates the mechanisms by which these eddies
382 regulate the production processes of NMHCs. Compared to the reference site, convergence in the surface
383 seawater within the anticyclonic eddy enhanced ocean stratification, which reduced nutrient availability
384 and consequently suppressed phytoplankton growth, leading to decreased concentrations of alkanes and
385 isoprene. For C₂-C₄ alkenes, the reduced photochemical production rates within the anticyclonic eddy
386 served as the key driver for their depressed concentrations in this mesoscale system. Regarding vertical
387 distribution, the peak concentrations of alkanes and isoprene typically occurred at deeper depths with the
388 eddy core. Driven by the anticyclonic eddy, variations in phytoplankton biomass played a key role in
389 shaping the spatial distributions of these NMHCs. In contrast, C₂-C₄ alkenes exhibited no sinking
390 behavior due to the limitation of light radiation. The calculated sea-to-air fluxes indicated that NMHC
391 emissions from the surface seawater of northern SCS made a substantial contribution to the global
392 NMHC inventory. However, the anticyclonic eddy suppressed the emission of NMHCs, reduced the SOA
393 formation potential, and consequently diminished their negative feedback effect on global warming. This
394 study highlights that understanding the mechanisms by which mesoscale dynamical processes influence
395 the distributions and emissions of NMHCs in seawater is essential to assessing the climate-sensitivity of
396 marine NMHC cycling.

397 **Data availability**

398 Data presented in this paper are publicly available on Figshare via
399 <https://doi.org/10.6084/m9.figshare.31007650> (Liu, 2026).

400 **Supplement link**

401 The supplement related to this article is available online.



402 **Author contributions**

403 Z-F.L.: Writing–review & editing, Writing–original draft, Investigation, Data curation, Visualization,
404 Conceptualization; W-Z.Q.: Writing–review & editing, Data curation, Conceptualization; Z-Y.Y.:
405 Writing–review & editing; F.X.: Writing–review & editing, Data curation, Conceptualization; G-B.X.:
406 Writing–review & editing; J.W.: Writing–review & editing, Data curation, Conceptualization, Funding
407 acquisition; H.Q.: Writing–review & editing, Conceptualization; C-S.L.: Writing–review & editing; H-
408 H. Z.: Writing–review & editing, Supervision, Resources, Funding acquisition, Conceptualization.

409 **Competing interests**

410 The contact author has declared that none of the authors has any competing interests.

411 **Disclaimer**

412 Publisher’s note: Copernicus Publications remains neutral with regard to jurisdictional claims made in
413 the text, published maps, institutional affiliations, or any other geographical representation in this paper.
414 The authors bear the ultimate responsibility for providing appropriate place names. Views expressed in
415 the text are those of the authors and do not necessarily reflect the views of the publisher.

416 **Acknowledgements**

417 We sincerely thank the chief scientist of the open research cruise NORC2021-05 and all crew members
418 of R/V “*Dongfanghong 3*” for their assistance in sampling and providing the CTD data.

419 **Financial support**

420 This work was supported by the National Natural Science Foundation of China (grant numbers 42576041,
421 42506044, and 42276042), the Laoshan National Laboratory Science and Technology Innovation
422 Program Project (LSKJ202400202 and LSKJ202201701), the Fundamental Research Funds for the
423 Central Universities (202572001 and 842513018), and the General Program of China Postdoctoral
424 Science Foundation (2025M770876).



425 **References**

- 426 An, L., Liu, X., Xu, F., Fan, X., Wang, P., Yin, W., and Huang, B.: Different responses of plankton
427 community to mesoscale eddies in the western equatorial Pacific Ocean, *Deep-Sea Res. Pt. I*, 203,
428 104219, <https://doi.org/10.1016/j.dsr.2023.104219>, 2024.
- 429 Atkinson, R.: Atmospheric chemistry of VOCs and NO_x, *Atmos. Environ.*, 34, 2063–2101,
430 [https://doi.org/10.1016/S1352-2310\(99\)00460-4](https://doi.org/10.1016/S1352-2310(99)00460-4), 2000.
- 431 Atkinson, R. and Arey, J.: Atmospheric degradation of volatile organic compounds, *Chem. Rev.*, 103,
432 4605–4638, <https://doi.org/10.1021/cr0206420>, 2003.
- 433 Bird, R. E. and Riordan, C.: Simple solar spectral model for direct and diffuse irradiance on horizontal
434 and tilted planes at the Earth's surface for cloudless atmospheres, *Journal of Climate and Applied
435 Meteorology*, 25, 87–97, <https://www.jstor.org/stable/26182461>, 1986.
- 436 Broadgate, W. J., Malin, G., Küpper, F. C., Thompson, A., and Liss, P. S.: Isoprene and other non-methane
437 hydrocarbons from seaweeds: a source of reactive hydrocarbons to the atmosphere, *Mar. Chem.*, 88,
438 61–73, <https://doi.org/10.1016/j.marchem.2004.03.002>, 2004.
- 439 Carpenter, L. J., Archer, S. D., and Beale, R.: Ocean-atmosphere trace gas exchange, *Chem. Soc. Rev.*,
440 41, 6473–6506, <https://doi.org/10.1039/C2CS35121H>, 2012.
- 441 Carter, W. P. L.: Development of the SAPRC-07 chemical mechanism, *Atmos. Environ.*, 44, 5324–5335,
442 <https://doi.org/10.1016/j.atmosenv.2010.01.026>, 2010.
- 443 Dacre, H. F., Gray, S. L., and Belcher, S. E.: A case study of boundary layer ventilation by convection
444 and coastal processes, *J. Geophys. Res.-Atmos.*, 112, <https://doi.org/10.1029/2006JD007984>, 2007.
- 445 Dai, S., Zhao, Y., Liu, H., Hu, Z., Zheng, S., Zhu, M., Guo, S., and Sun, X.: The effects of a warm-core
446 eddy on chlorophyll *a* distribution and phytoplankton community structure in the northern South China
447 Sea in spring 2017, *J. Mar. Syst.*, 210, 103396, <https://doi.org/10.1016/j.jmarsys.2020.103396>, 2020.
- 448 Dani, K. G. S. and Loreto, F.: Trade-off between dimethyl sulfide and isoprene emissions from marine
449 phytoplankton, *Trends Plant Sci.*, 22, 361–372, <https://doi.org/10.1016/j.tplants.2017.01.006>, 2017.
- 450 Derwent, R. G., Jenkin, M. E., Utembe, S. R., Shallcross, D. E., Murrells, T. P., and Passant, N. R.:
451 Secondary organic aerosol formation from a large number of reactive man-made organic compounds,
452 *Sci. Total Environ.*, 408, 3374–3381, <https://doi.org/10.1016/j.scitotenv.2010.04.013>, 2010.



- 453 Ding, X., Wang, X., Xie, Z., Zhang, Z., and Sun, L.: Impacts of siberian biomass burning on organic
454 aerosols over the north Pacific Ocean and the Arctic: primary and secondary organic tracers, *Environ.*
455 *Sci. Technol.*, 47, 3149–3157, <https://doi.org/10.1021/es3037093>, 2013.
- 456 Gist, N. and Lewis, A. C.: Seasonal variations of dissolved alkenes in coastal waters, *Mar. Chem.*, 100,
457 1–10, <https://doi.org/10.1016/j.marchem.2005.10.004>, 2006.
- 458 Hallquist, M., Wenger, J. C., Baltensperger, U., Rudich, Y., Simpson, D., Claeys, M., Dommen, J.,
459 Donahue, N. M., George, C., Goldstein, A. H., Hamilton, J. F., Herrmann, H., Hoffmann, T., Iinuma,
460 Y., Jang, M., Jenkin, M. E., Jimenez, J. L., Kiendler-Scharr, A., Maenhaut, W., McFiggans, G., Mentel,
461 T. F., Monod, A., Prévôt, A. S. H., Seinfeld, J. H., Surratt, J. D., Szmigielski, R., and Wildt, J.: The
462 formation, properties and impact of secondary organic aerosol: current and emerging issues, *Atmos.*
463 *Chem. Phys.*, 9, 5155–5236, <https://doi.org/10.5194/acp-9-5155-2009>, 2009.
- 464 Jia, Y. and Chassignet, E. P.: Seasonal variation of eddy shedding from the Kuroshio intrusion in the
465 Luzon Strait, *J Oceanogr*, 67, 601–611, <https://doi.org/10.1007/s10872-011-0060-1>, 2011.
- 466 Jobson, B. T., McKeen, S. A., Parrish, D. D., Fehsenfeld, F. C., Blake, D. R., Goldstein, A. H., Schauffler,
467 S. M., and Elkins, J. W.: Trace gas mixing ratio variability versus lifetime in the troposphere and
468 stratosphere: observations, *J. Geophys. Res.-Atmos.*, 104, 16091–16113,
469 <https://doi.org/10.1029/1999JD900126>, 1999.
- 470 Krechmer, J. E., Coggon, M. M., Massoli, P., Nguyen, T. B., Crounse, J. D., Hu, W., Day, D. A., Tyndall,
471 G. S., Henze, D. K., Rivera-Rios, J. C., Nowak, J. B., Kimmel, J. R., Mauldin, R. L. I., Stark, H., Jayne,
472 J. T., Sipilä, M., Junninen, H., St. Clair, J. M., Zhang, X., Feiner, P. A., Zhang, L., Miller, D. O., Brune,
473 W. H., Keutsch, F. N., Wennberg, P. O., Seinfeld, J. H., Worsnop, D. R., Jimenez, J. L., and Canagaratna,
474 M. R.: Formation of low volatility organic compounds and secondary organic aerosol from isoprene
475 hydroxyhydroperoxide low-NO oxidation, *Environ. Sci. Technol.*, 49, 10330–10339,
476 <https://doi.org/10.1021/acs.est.5b02031>, 2015.
- 477 Lee, R. F. and Baker, J.: Ethylene and ethane production in an estuarine river: formation from the
478 decomposition of polyunsaturated fatty acids, *Mar. Chem.*, 38, 25–36, [https://doi.org/10.1016/0304-](https://doi.org/10.1016/0304-4203(92)90065-I)
479 [4203\(92\)90065-I](https://doi.org/10.1016/0304-4203(92)90065-I), 1992.



- 480 Li, J. L., Zhai, X., Ma, Z., Zhang, H. H., and Yang, G. P.: Spatial distributions and sea-to-air fluxes of
481 non-methane hydrocarbons in the atmosphere and seawater of the Western Pacific Ocean, *Sci. Total*
482 *Environ.*, 672, 491–501, <https://doi.org/10.1016/j.scitotenv.2019.04.019>, 2019.
- 483 Li, J. L., Zhai, X., Wu, Y. C., Wang, J., Zhang, H. H., and Yang, G. P.: Emissions and potential controls
484 of light alkenes from the marginal seas of China, *Sci. Total Environ.*, 758, 143655,
485 <https://doi.org/10.1016/j.scitotenv.2020.143655>, 2021.
- 486 Liang, Q., Wang, C., Li, Y., Xie, X., Guo, X., Liu, X., Wang, W., Zhang, Z., and Guo, W.: Kuroshio-
487 derived anticyclonic eddies drive lateral transport and transformation of oceanic dissolved organic
488 matter along the continental slope of South China Sea, *J. Geophys. Res.-Oceans*, 130, e2024JC021718,
489 <https://doi.org/10.1029/2024JC021718>, 2025.
- 490 Lin, X., Dong, C., Chen, D., Liu, Y., Yang, J., Zou, B., and Guan, Y.: Three-dimensional properties of
491 mesoscale eddies in the South China Sea based on eddy-resolving model output, *Deep-Sea Res. Pt. I*,
492 99, 46–64, <https://doi.org/10.1016/j.dsr.2015.01.007>, 2015.
- 493 Liu, H., Zhu, M., Guo, S., Zhao, X., and Sun, X.: Effects of an anticyclonic eddy on the distribution and
494 community structure of zooplankton in the South China Sea northern slope, *J. Mar. Syst.*, 205, 103311,
495 <https://doi.org/10.1016/j.jmarsys.2020.103311>, 2020.
- 496 Liu, Z.: Impact of anticyclonic eddies on the spatial distribution and emission of non-methane
497 hydrocarbons in the northern South China Sea, Figshare [data set],
498 <https://doi.org/10.6084/m9.figshare.31007650>, 2026.
- 499 Luo, G. and Yu, F.: A numerical evaluation of global oceanic emissions of α -pinene and isoprene, *Atmos.*
500 *Chem. Phys.*, 10, 2007–2015, <https://doi.org/10.5194/acp-10-2007-2010>, 2010.
- 501 McGillicuddy, D. J.: Mechanisms of physical-biological-biogeochemical interaction at the oceanic
502 mesoscale, *Annu. Rev. Mar. Sci.*, 8, 125–159, <https://doi.org/10.1146/annurev-marine-010814-015606>,
503 2016.
- 504 McGillicuddy, D. J., Robinson, A. R., Siegel, D. A., Jannasch, H. W., Johnson, R., Dickey, T. D., McNeil,
505 J., Michaels, A. F., and Knap, A. H.: Influence of mesoscale eddies on new production in the Sargasso
506 Sea, *Nature*, 394, 263–266, <https://doi.org/10.1038/28367>, 1998.



- 507 McGillicuddy, D. J., Anderson, L. A., Bates, N. R., Bibby, T., Buesseler, K. O., Carlson, C. A., Davis, C.
508 S., Ewart, C., Falkowski, P. G., Goldthwait, S. A., Hansell, D. A., Jenkins, W. J., Johnson, R., Kosnyrev,
509 V. K., Ledwell, J. R., Li, Q. P., Siegel, D. A., and Steinberg, D. K.: Eddy/wind interactions stimulate
510 extraordinary mid-ocean plankton blooms, *Science*, 316, 1021–1026,
511 <https://doi.org/10.1126/science.1136256>, 2007.
- 512 McKay, W. A., Turner, M. F., Jones, B. M. R., and Halliwell, C. M.: Emissions of hydrocarbons from
513 marine phytoplankton—Some results from controlled laboratory experiments, *Atmos. Environ.*, 30,
514 2583–2593, [https://doi.org/10.1016/1352-2310\(95\)00433-5](https://doi.org/10.1016/1352-2310(95)00433-5), 1996.
- 515 Men, G., Wan, X., and Ma, W.: The vertical tilt of mesoscale eddy in the northern South China Sea in a
516 high-resolution numerical simulation, *J. Geophys. Res.-Oceans*, 129, e2024JC021083,
517 <https://doi.org/10.1029/2024JC021083>, 2024.
- 518 Messina, P., Lathière, J., Sindelarova, K., Vuichard, N., Granier, C., Ghattas, J., Cozic, A., and
519 Hauglustaine, D. A.: Global biogenic volatile organic compound emissions in the ORCHIDEE and
520 MEGAN models and sensitivity to key parameters, *Atmos. Chem. Phys.*, 16, 14169–14202,
521 <https://doi.org/10.5194/acp-16-14169-2016>, 2016.
- 522 Panda, U., Mahapatra, P. S., and Das, T.: Study of C2–C5 non-methane hydrocarbons and their ozone
523 formation potential at Bhubaneswar, an eastern coastal site in India, *MAPAN*, 30, 195–202,
524 <https://doi.org/10.1007/s12647-015-0134-4>, 2015.
- 525 Plass-Dülmer, C., Khedim, A., Koppmann, R., Johnen, F. J., Rudolph, J., and Kuosa, H.: Emissions of
526 light nonmethane hydrocarbons from the Atlantic into the atmosphere, *Global Biogeochem. Cy.*, 7,
527 211–228, <https://doi.org/10.1029/92GB02361>, 1993.
- 528 Qiao, W. Z., Wu, Y. C., Wang, P., Wang, J., Zhou, L. M., Li, S. T., and Zhang, H. H.: Distribution
529 characteristics and environmental effects of non-methane hydrocarbons in the East China Sea, *Cont.*
530 *Shelf Res.*, 261, 105023, <https://doi.org/10.1016/j.csr.2023.105023>, 2023.
- 531 Ratte, M., Plass-Dülmer, C., Koppmann, R., Rudolph, J., and Denga, J.: Production mechanism of C2-
532 C4 hydrocarbons in seawater: Field measurements and experiments, *Global Biogeochem. Cy.*, 7, 369–
533 378, <https://doi.org/10.1029/93GB00054>, 1993.



- 534 Ratte, M., Bujok, O., Spitzzy, A., and Rudolph, J.: Photochemical alkene formation in seawater from
535 dissolved organic carbon: Results from laboratory experiments, *J. Geophys. Res.-Atmos.*, 103, 5707–
536 5717, <https://doi.org/10.1029/97JD03473>, 1998.
- 537 Riva, M., Budisulistiorini, S. H., Zhang, Z., Gold, A., and Surratt, J. D.: Chemical characterization of
538 secondary organic aerosol constituents from isoprene ozonolysis in the presence of acidic aerosol,
539 *Atmos. Environ.*, 130, 5–13, <https://doi.org/10.1016/j.atmosenv.2015.06.027>, 2016.
- 540 Shih, Y. Y., Hung, C. C., Tuo, S., Shao, H. J., Chow, C. H., Muller, F. L. L., and Cai, Y. H.: The impact
541 of eddies on nutrient supply, diatom biomass and carbon export in the northern South China Sea, *Front.*
542 *Earth Sci.*, 8, 537332, <https://doi.org/10.3389/feart.2020.537332>, 2020.
- 543 Song, J., Zhao, Y., Zhang, Y., Fu, P., Zheng, L., Yuan, Q., Wang, S., Huang, X., Xu, W., Cao, Z., Gromov,
544 S., and Lai, S.: Influence of biomass burning on atmospheric aerosols over the western South China
545 Sea: Insights from ions, carbonaceous fractions and stable carbon isotope ratios, *Environ. Pollut.*, 242,
546 1800–1809, <https://doi.org/10.1016/j.envpol.2018.07.088>, 2018.
- 547 Song, J., Zhang, Y., Zhang, Y., Yuan, Q., Zhao, Y., Wang, X., Zou, S., Xu, W., and Lai, S.: A case study
548 on the characterization of non-methane hydrocarbons over the South China Sea: Implication of land-
549 sea air exchange, *Sci. Total Environ.*, 717, 134754, <https://doi.org/10.1016/j.scitotenv.2019.134754>,
550 2020.
- 551 Sweeney, E. N., McGillicuddy, D. J., and Buesseler, K. O.: Biogeochemical impacts due to mesoscale
552 eddy activity in the Sargasso Sea as measured at the Bermuda Atlantic Time-series Study (BATS),
553 *Deep-Sea Res. Pt. II*, 50, 3017–3039, <https://doi.org/10.1016/j.dsr2.2003.07.008>, 2003.
- 554 Tian, J., Zhang, Y., Jing, H., Ren, H., Mao, H., Zhou, H., Zheng, M., Chen, M., Zhang, R., and Chen, M.:
555 Reshaping of new nitrogen regime by anticyclonic eddies in the northern South China Sea, *J. Geophys.*
556 *Res.-Oceans*, 130, e2024JC021684, <https://doi.org/10.1029/2024JC021684>, 2025.
- 557 Tran, S., Bonsang, B., Gros, V., Peeken, I., Sarda-Esteve, R., Bernhardt, A., and Belviso, S.: A survey of
558 carbon monoxide and non-methane hydrocarbons in the Arctic Ocean during summer 2010,
559 *Biogeosciences*, 10, 1909–1935, <https://doi.org/10.5194/bg-10-1909-2013>, 2013.



- 560 Wang, J., Zhang, H. H., Booge, D., Zhang, Y. Q., Li, X. J., Wu, Y. C., Zhang, J. W., and Chen, Z. H.:
561 Isoprene production and its driving factors in the northwest Pacific Ocean, *Global Biogeochem. Cy.*,
562 37, e2023GB007841, <https://doi.org/10.1029/2023GB007841>, 2023.
- 563 Wang, J., Xue, L., Ma, Q., Xu, F., Xu, G., Yan, S., Zhang, J., Li, J., Zhang, H., Zhang, G., and Chen, Z.:
564 The role of oceanic ventilation and terrestrial outflow in atmospheric non-methane hydrocarbons over
565 the Chinese marginal seas, *Atmos. Chem. Phys.*, 24, 8721–8736, [https://doi.org/10.5194/acp-24-8721-](https://doi.org/10.5194/acp-24-8721-2024)
566 2024, 2024.
- 567 Wanninkhof, R.: Relationship between wind speed and gas exchange over the ocean, *J. Geophys. Res.-*
568 *Oceans*, 97, 7373–7382, <https://doi.org/10.1029/92JC00188>, 1992.
- 569 Wanninkhof, R.: Relationship between wind speed and gas exchange over the ocean revisited, *Limnol.*
570 *Oceanogr.: Methods*, 12, 351–362, <https://doi.org/10.4319/lom.2014.12.351>, 2014.
- 571 Wilke, C. R. and Chang, P.: Correlation of diffusion coefficients in dilute solutions, *AIChE Journal*, 1,
572 264–270, <https://doi.org/10.1002/aic.690010222>, 1955.
- 573 Wu, Y. C., Li, J. L., Wang, J., Zhuang, G. C., Liu, X. T., Zhang, H. H., and Yang, G. P.: Occurance,
574 emission and environmental effects of non-methane hydrocarbons in the Yellow Sea and the East
575 China Sea, *Environ. Pollut.*, 270, 116305, <https://doi.org/10.1016/j.envpol.2020.116305>, 2021.
- 576 Wu, Y. C., Gao, X. X., Zhang, H. H., Liu, Y. Z., Wang, J., Xu, F., Zhang, G. L., and Chen, Z. H.:
577 Characteristics and emissions of isoprene and other non-methane hydrocarbons in the Northwest
578 Pacific Ocean and responses to atmospheric aerosol deposition, *Sci. Total Environ.*, 876, 162808,
579 <https://doi.org/10.1016/j.scitotenv.2023.162808>, 2023.
- 580 Yuan, Q., Lai, S., Song, J., Ding, X., Zheng, L., Wang, X., Zhao, Y., Zheng, J., Yue, D., Zhong, L., Niu,
581 X., and Zhang, Y.: Seasonal cycles of secondary organic aerosol tracers in rural Guangzhou, Southern
582 China: The importance of atmospheric oxidants, *Environ. Pollut.*, 240, 884–893,
583 <https://doi.org/10.1016/j.envpol.2018.05.009>, 2018.
- 584 Zhang, H. H., Li, J. L., Yang, G. P., Song, Y. C., and Jin, N.: Purge-trap gas chromatography and mass
585 spectrometric method for analysis of isoprene in natural waters, *Chin. J. Anal. Chem.*, 43, 333–337,
586 [https://doi.org/10.1016/S1872-2040\(15\)60812-X](https://doi.org/10.1016/S1872-2040(15)60812-X), 2015.



- 587 Zhang, W., Zhang, C., Zheng, S., Chen, Y., Zhu, M., and Sun, X.: Distribution of picophytoplankton in
588 the northern slope of the South China Sea under environmental variation induced by a warm eddy,
589 *Mar. Pollut. Bull.*, 194, 115429, <https://doi.org/10.1016/j.marpolbul.2023.115429>, 2023.
- 590 Zhang, Z., Wang, H., Chen, D., Li, Q., Thai, P., Gong, D., Li, Y., Zhang, C., Gu, Y., Zhou, L., Morawska,
591 L., and Wang, B.: Emission characteristics of volatile organic compounds and their secondary organic
592 aerosol formation potentials from a petroleum refinery in Pearl River Delta, China, *Sci. Total Environ.*,
593 584–585, 1162–1174, <https://doi.org/10.1016/j.scitotenv.2017.01.179>, 2017.
- 594 Zhou, K., Dai, M., Kao, S.-J., Wang, L., Xiu, P., Chai, F., Tian, J., and Liu, Y.: Apparent enhancement of
595 ²³⁴Th-based particle export associated with anticyclonic eddies, *Earth Planet. Sci. Lett.*, 381, 198–
596 209, <https://doi.org/10.1016/j.epsl.2013.07.039>, 2013.
- 597 Zhou, K., Dai, M., Xiu, P., Wang, L., Hu, J., and Benitez-Nelson, C. R.: Transient enhancement and
598 decoupling of carbon and opal export in cyclonic eddies, *J. Geophys. Res.-Oceans*, 125,
599 e2020JC016372, <https://doi.org/10.1029/2020JC016372>, 2020.
- 600 Zhou, K., Xu, Y., Kao, S. J., Xiu, P., Wan, X., Huang, B., Liu, X., Du, C., Sun, J., Sun, Z., and Dai, M.:
601 Changes in nutrient stoichiometry in responding to diatom growth in cyclonic eddies, *Geosci. Lett.*,
602 10, 12, <https://doi.org/10.1186/s40562-023-00269-8>, 2023.
- 603